Available online at www.sciencedirect.com
ScienceDirect
Physics Letters A 372 (2008) 3210–3216
PHYSICS LETTERS A
www.elsevier.com/locate/pla

Self focusing of acoustically excited Faraday ripples on a bubble wall

Alexey O. Maksimov [a,*], Timothy G. Leighton [b], Peter R. Birkin [c]

[a] V.I. Il'ichev's Pacific Oceanological Institute, Far Eastern Branch of the Russian Academy of Sciences, Vladivostok 690041, Russia
[b] Institute of Sound and Vibration Research, University of Southampton, Highfield, Southampton SO17 1BJ, UK
[c] School of Chemistry, University of Southampton, Highfield, Southampton SO17 1BJ, UK

Received 18 October 2007; received in revised form 17 January 2008; accepted 24 January 2008

Available online 1 February 2008

Communicated by A.P. Fordy

Abstract

A theoretical explanation is presented to explain pattern formation during the generation of Faraday waves on a bubble wall. The theory derives the Hamiltonian formulation of the nonlinear bubble dynamics. The nonlinear Schrödinger equation for the envelope of surface modes on the bubble wall has been obtained. The solitary wave solution predicts that the shape distortions should be localized near the equator of the bubble.

Keywords: Bubble; Faraday ripples; Hamiltonian dynamics; Solitary wave

1. Introduction

The following investigation was stimulated by observations of standing surface waves on the wall of a bubble which is subjected to an acoustical field at a frequency of approximately twice the natural frequency of these distortion modes [1–3]. These studies demonstrate that a wave train of Faraday ripples can be located near the equator of the bubble, and that the width of this wave train in the direction of the zenith angle ϑ is smaller than the bubble diameter, but larger than the wave period $2\pi R_0/n$ (we use the spherical coordinates (r, ϑ, α) with the equation of the bubble surface as $r = R \equiv R_0 + \xi(\vartheta, \alpha, t)$, where R, R_0 are the instantaneous and equilibrium bubble radii, and n is the mode number). One of the possible explanations for the localization of the wave train in the ϑ-direction is self-focusing of the ripples.

In the 1980s, Wu et al. [4] observed a solitary wave in a long channel subjected to a vertical oscillation at a frequency of approximately twice the natural frequency of the dominant cross-wave (see Fig. 1). Miles [5] and Larraza and Putterman [6] derived theory describing this effect. A close analogy can be established between the generation of Faraday ripples in a channel and on the bubble wall. The following analysis exploits that analogy.

2. Hamiltonian formalism in bubble dynamics

Consider the irrotational motion of an incompressible inviscid fluid near the bubble wall. The velocity potential, denoted by φ, is governed by the Laplace's equation

$$\nabla^2\varphi = 0, \qquad \mathbf{v} = \nabla\varphi, \tag{1}$$

where $\mathbf{v}$ is the velocity. The kinematic boundary condition at the bubble wall takes the form

$$\big[\partial/\partial t + (\mathbf{v}, \nabla)\big](r - R)_{r=R_0+\xi} = 0. \tag{2}$$

* Corresponding author.
E-mail address: maksimov@poi.dvo.ru (A.O. Maksimov).

0375-9601/$ – see front matter
doi:10.1016/j.physleta.2008.01.041

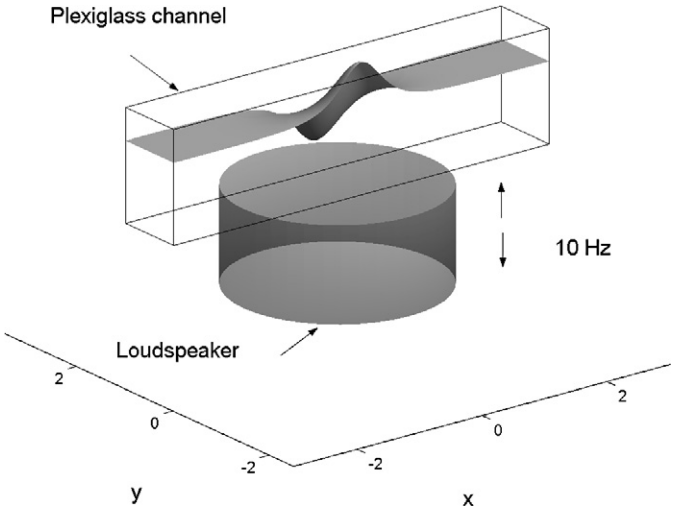

Fig. 1. The shape of the solitary wave in a channel [4]. Waves were generated by placing the horizontal trough on a loudspeaker driven at a frequency 10 Hz.

The dynamical boundary condition describes how the pressures on the two sides of the surface differ only because of surface tension, i.e., if P_l and P_g denote the pressure in the water and in the bubble correspondingly, then

$$P_l = P_g - \sigma(\nabla, \mathbf{n}), \quad P_g = P_0(V_0/V)^\gamma, \tag{3}$$

where σ is the coefficient of the surface tension and $\mathbf{n}$ is the unit vector normal to the surface $r = R_0 + \xi(\vartheta, \alpha, t)$. We adopt a polytropic law for the gas bubble where V, V_0 are the instantaneous and equilibrium bubble volumes respectively, γ is the polytropic exponent, P_0 is equilibrium gas pressure in the bubble and P_l is governed by the first integral of the potential flow

$$P_l = -\rho_0\left[\frac{\partial\varphi}{\partial t} + \frac{(\nabla\varphi)^2}{2}\right] + P_\infty,$$

where ρ_0 is the equilibrium density and P_∞ is the external pressure in the liquid far from the bubble (which can contain both steady and unsteady components).

The investigation of non-stationary irrotational flows in a space region D with free surface S can be reduced to the consideration of Hamiltonian dynamics of the surface [7–9]. In this formulation, the shape of the surface S itself and the boundary value $\Phi = \varphi(r, \vartheta, \alpha, t)|_{r=R_0+\xi}$ of the velocity potential are the dynamical variables determining the state of the system. That is, for each time t, the wall displacement function $\xi(\vartheta, \alpha, t)$ determines the domain occupied by the liquid, and the velocity potential on the bubble wall $\Phi(\vartheta, \alpha, t)$ determines the corresponding velocity potential elsewhere $\varphi(r, \vartheta, \alpha, t)$, the latter being the unique solution of the linear boundary-value problem described by (1) and $\varphi(r, \vartheta, \alpha, t)|_{r=R_0+\xi} = \Phi(\vartheta, \alpha, t)$.

The problem is amenable to a Hamiltonian formulation with the Hamiltonian

$$\begin{aligned}
&H = T + U + A, \quad U = V_{\text{in}} + V_s,\\
&T = \rho_0 \iiint \frac{\mathbf{v}^2}{2}\, d\mathbf{r}, \quad V_{\text{in}} = -\int P_g\, dV = -\frac{P_0 V_0}{(\gamma-1)}\left(\frac{V_0}{V}\right)^{\gamma-1}, \quad A = P_\infty(V - V_0),\\
&V_s = \sigma \iint J(R_0+\xi)^2 \sin\vartheta\, d\vartheta\, d\alpha, \quad J^2 = \left[1 + \frac{1}{(R_0+\xi)^2}\left(\frac{\partial\xi}{\partial\vartheta}\right)^2 + \frac{1}{(R_0+\xi)^2\sin^2\vartheta}\left(\frac{\partial\xi}{\partial\alpha}\right)^2\right],
\end{aligned} \tag{4}$$

where T is the kinetic energy, U is the potential energy (which is the sum of the internal energy V_{in} and the surface energy V_s), the quantity $J(R_0+\xi)^2 \sin\vartheta\, d\vartheta\, d\alpha$ is the area element of the water surface, and the term A is the work done by the sound field on the bubble. The resulting canonical equations of motion are [9,10]

$$\frac{\partial\xi}{\partial t} = \frac{\delta H}{\delta \Pi}, \quad \frac{\partial \Pi}{\partial t} = -\frac{\delta H}{\delta\xi}, \quad \Pi = -\rho_0(R_0+\xi)^2\Phi(\vartheta, \alpha, t), \tag{5}$$

where $\delta/\delta\xi$, $\delta/\delta\Pi$ denote functional derivatives. These equations coincide with the kinematic and dynamic boundary conditions.

Unfortunately H cannot be written in the closed form as a functional of Π, ξ. However one can limit the Hamiltonian to the first few terms of an expansion in powers of Π, and ξ [11], as follows:

$$\begin{aligned}
&H = H_0 + H_1 + H_2 + \cdots,\\
&H_0 = \iint\left[\frac{\Pi\hat{D}(\Pi)}{2\rho_0 R_0^3} - \frac{\sigma R_0^2}{2} s\left(\nabla_s^2 s\right)\right]\sin\vartheta\, d\vartheta\, d\alpha + 6\pi\gamma\left(P_\infty + \frac{2\sigma}{R_0}\right)R_0^3\bar{s}^2 - 4\pi\sigma R_0^2\overline{s^2},
\end{aligned}$$

$$
\begin{aligned}
H_1 &= \frac{1}{2\rho_0 R_0^3}\iint s\big[(\hat{D}\Pi)^2 - (\nabla_s \Pi)^2 - 4\Pi\hat{D}(\Pi)\big]\sin\vartheta\, d\vartheta\, d\alpha \\
&\quad + 12\pi\gamma\left(P_\infty + \frac{2\sigma}{R_0}\right)R_0^3\bar{s}\left[\overline{s^2} - \frac{(\gamma+1)}{2}(\bar{s})^2\right] - \frac{8}{3}\pi\sigma R_0^2\overline{s^3}, \\
H_2 &= \iint\left\{\frac{1}{2\rho_0 R_0^3}\big[s\hat{D}(\Pi)\big[\hat{D}(s\hat{D}\Pi) + s\big(\nabla_s^2\Pi\big)\big] + s\big[4\big(\nabla_s(\Pi),\nabla_s(s\Pi)\big) - 4\hat{D}(\Pi)\hat{D}(s\Pi) - s\big(\hat{D}(\Pi)\big)^2\big]\right. \\
&\quad \left. - 2s\big[3s\Pi\hat{D}(\Pi) + 2\Pi\hat{D}(s\Pi)\big]\big] - \frac{\sigma R_0^2}{8}\left[\nabla_s^2\left(\frac{s^2}{2}\right) - s\big(\nabla_s^2 s\big)\right]^2\right\}\sin\vartheta\, d\vartheta\, d\alpha \\
&\quad + 4\pi\gamma\left(P_\infty + \frac{2\sigma}{R_0}\right)R_0^3\left[\overline{s^3}\bar{s} + \frac{3}{2}\big(\overline{s^2}\big)^2 - \frac{9(\gamma+1)}{2}(\bar{s})^2\overline{s^2} + \frac{9(\gamma+1)(\gamma+2)}{2}(\bar{s})^4\right],
\end{aligned}
\tag{6}
$$

where $s \equiv \xi/R_0$, $\bar{A} \equiv (4\pi)^{-1}\iint A\sin\vartheta\, d\vartheta\, d\alpha$, $\nabla_s \equiv \mathbf{e}_\vartheta\partial/\partial\vartheta + \sin^{-1}\vartheta\,\mathbf{e}_\alpha\partial/\partial\alpha$ is the surface gradient, and $\hat{D} = [(1/2) + \sqrt{-\nabla_s^2 + (1/4)}\,]$ is a linear operator.

The general method for analyzing a weakly nonlinear Hamiltonian system consists of carrying out a canonical transformation from Π, ξ to the normal variables, in which the quadratic Hamiltonian is diagonalized. In order to classify the nonlinear interaction between waves, subsequent terms in the expansion in powers of the normal coordinates can be obtained. Unfortunately, this general method leads to very cumbersome expressions (see [11]). For this reason we shall follow the more heuristic approach proposed in [6] and seek a perturbation (multiple scales) solution of Eqs. (5) of the form

$$
\begin{aligned}
&\xi(\vartheta,\alpha,t,\varepsilon,n) = \varepsilon\xi_1(\vartheta,\alpha,T_0,T_1,T_2,\ldots,n) + \varepsilon^2\xi_2(\vartheta,\alpha,T_0,T_1,T_2,\ldots,n) + \cdots, \\
&\Pi(\vartheta,\alpha,t,\varepsilon,n) = \varepsilon\Pi_1(\vartheta,\alpha,T_0,T_1,T_2,\ldots,n) + \varepsilon^2\Pi_2(\vartheta,\alpha,T_0,T_1,T_2,\ldots,n) + \cdots, \\
&\frac{\partial}{\partial t} = \frac{\partial}{\partial T_0} + \varepsilon\frac{\partial}{\partial T_1} + \varepsilon^2\frac{\partial}{\partial T_2} + \cdots.
\end{aligned}
$$

The parameter ε is related to the wave steepness by the formula $\varepsilon = (n\xi/\pi R_0)$. We are interested in the weakly nonlinear problem of a disturbance with a high frequency of motion ω in the α-direction (along the bubble equator) modulated by an envelope $\tilde{\xi}_1(\vartheta,t)$ in the ϑ-direction (along the meridian)

$$
\xi_1(\vartheta,\alpha,T_0,T_1,T_2,\ldots,n) = \frac{1}{2}\big[\tilde{\xi}_1(\vartheta,T_1,T_2,\ldots,n)e^{-i\omega T_0} + \text{c.c.}\big]\cos(n\alpha).
$$

By substituting the expansion for the Hamiltonian into the canonical equations of motion, we have

$$
\begin{aligned}
&\left(\frac{\partial}{\partial T_0} + \varepsilon\frac{\partial}{\partial T_1} + \varepsilon^2\frac{\partial}{\partial T_2} + \cdots\right)\big[\varepsilon\xi_1 + \varepsilon^2\xi_2 + \cdots\big] = \frac{1}{\rho_0 R_0^3}\hat{D}\big[\varepsilon\Pi_1 + \varepsilon^2\Pi_2 + \cdots\big] + \{\cdots\}, \\
&\left(\frac{\partial}{\partial T_0} + \varepsilon\frac{\partial}{\partial T_1} + \varepsilon^2\frac{\partial}{\partial T_2} + \cdots\right)\big[\varepsilon\Pi_1 + \varepsilon^2\Pi_2 + \cdots\big] = \sigma\big(\nabla_s^2 + 2\big)\big[\varepsilon\xi_1 + \varepsilon^2\xi_2 + \cdots\big] + \{\cdots\}.
\end{aligned}
$$

Retaining only terms of order ε we obtain

$$
\begin{aligned}
&-\frac{i\omega}{2}\big(\tilde{\xi}_1 e^{-i\omega T_0} - \text{c.c.}\big)\cos(n\alpha) = \frac{\hat{D}(\Pi_1)}{\rho_0 R_0^3}, \qquad \frac{\partial\Pi_1}{\partial T_0} = \frac{\sigma}{2}\big(\nabla_s^2 + 2\big)\big(\tilde{\xi}_1 e^{-i\omega T_0} + \text{c.c.}\big)\cos(n\alpha), \\
&\Pi_1 = -\sigma\big(\nabla_s^2 + 2\big)\frac{1}{2i\omega}\big(\tilde{\xi}_1 e^{-i\omega T_0} + \text{c.c.}\big)\cos(n\alpha), \\
&\left[-\omega^2 - \frac{\sigma}{\rho_0 R_0^3}\hat{D}\big(\nabla_s^2 + 2\big)\right]\tilde{\xi}_1(\vartheta)\cos(n\alpha) = 0.
\end{aligned}
\tag{7}
$$

To the lowest order, the frequency is uniquely determined by the value of n through the dispersion relation

$$
\omega_1^2 = \sigma_n^2 \approx \frac{\sigma n^3}{\rho_0 R_0^3},
\tag{8}
$$

where $\sigma_n = \sqrt{\sigma(n+1)(n+2)(n-1)(\rho_0 R_0^3)^{-1}}$ is the natural frequency of the surface mode, an expression which reduces to $\sigma_n = \sqrt{\sigma n^3(\rho_0 R_0^3)^{-1}}$ if, as is the case for the Faraday waves observed experimentally in this study (Fig. 2), the mode number n relating to the Faraday wave is greater than about 10. The surface modes are quite dense for large n. In particular, the frequency separation between adjacent modes $\sigma_{n+1} - \sigma_n \approx (3/2)(\sigma_n/n)$ can be smaller than the resonance mismatch $|\omega - \omega_1|$.

Following Larraza and Putterman [6] we seek solutions where the variations of the physical quantities are described by

$$\frac{\omega_1^2}{\omega^2} - 1 = O\left(\varepsilon^2\right) \quad \text{(a)}, \qquad \frac{1}{n\tilde{\xi}_1}\frac{\partial\tilde{\xi}_1}{\partial\vartheta} = O(\varepsilon) \quad \text{(b)}, \qquad \frac{1}{\omega\tilde{\xi}_1}\frac{\partial\tilde{\xi}_1}{\partial t} = O(\varepsilon) \quad \text{(c)}. \tag{9}$$

Condition (9a) implies that the phase velocity (which is determined by the motion along the equator) and group velocity (which is determined by the envelope and leads to the presence of dispersion) are orthogonal in the main order magnitude. Conditions (9b), (9c) imply steepness of the envelope along the meridian and with time respectively. These assumptions are verified at the end of these calculations and greatly simplify the calculations when compared to the general method of canonical transformations. As the present work is based on a physical analogy between the structure of the Faraday ripples in a channel and on a bubble wall, identical methods of calculation were applied to demonstrate that they are actually similar.

We can now evaluate the dispersion of the wave packet on the sphere describing the envelope $\tilde{\xi}_1(\vartheta)$

$$\begin{aligned}\frac{\sigma}{\rho_0 R_0^3}\hat{D}\left(\nabla_s^2+2\right)\tilde{\xi}_1(\vartheta)\cos(n\alpha) &= \frac{\sigma}{\rho_0 R_0^3}\left[(1/2)+\sqrt{-\nabla_s^2+(1/4)}\,\right]\left(\nabla_s^2+2\right)\tilde{\xi}_1(\vartheta)\cos(n\alpha)\\ &= \frac{\sigma n^3}{\rho_0 R_0^3}\left[1+\frac{5}{8n}+\frac{3}{2}x^2-\frac{3}{2n^2}\frac{\partial^2}{\partial x^2}\right]\tilde{\xi}_1(\vartheta)\cos(n\alpha), \quad x=\cos\vartheta,\end{aligned}$$

and transform the contribution of the terms obtained in the first approximation (7) to

$$\omega^2\left[\left(\frac{\omega_1^2}{\omega^2}-1\right)+\left(\frac{5}{8n}+\frac{3}{2}x^2\right)-\frac{3}{2n^2}\frac{\partial^2}{\partial x^2}\right]\tilde{\xi}_1(\vartheta)\cos(n\alpha). \tag{10}$$

According to the conditions (9) the frequency mismatch and the dispersion are small and contribute only at the higher approximations.

To the next order, one finds

$$\begin{aligned}&\frac{\partial}{\partial T_0}\xi_2(\vartheta,\alpha,T_0,T_1,\ldots,n)+\frac{\partial}{\partial T_1}\frac{1}{2}\left(\tilde{\xi}_1 e^{-i\omega T_0}+\text{c.c.}\right)\cos(n\alpha)\\ &\quad=\frac{1}{\rho_0 R_0^3}\left[\hat{D}(\Pi_2)+\hat{D}\left(s_1\hat{D}(\Pi_1)\right)+(\nabla_s,s_1\nabla_s\Pi_1)-2s_1\hat{D}(\Pi_1)-2\hat{D}(s_1\Pi_1)\right],\\ &\frac{\partial}{\partial T_0}\Pi_2(\vartheta,\alpha,T_0,T_1,\ldots,n)+\frac{\partial}{\partial T_1}\frac{1}{2}\left(\Pi_1 e^{-i\omega T_0}+\text{c.c.}\right)\cos(n\alpha)\\ &\quad=\sigma\left(\nabla_s^2+2\right)\xi_2+2\sigma R_0 s_1^2-3\gamma\left(P_\infty+\frac{2\sigma}{R_0}\right)R_0^2\left(\bar{s}_2+\overline{s_1^2}\right)-\frac{1}{2\rho_0 R_0^4}\left[\left(\hat{D}(\Pi_1)\right)^2-(\nabla_s\Pi_1)^2-4\Pi_1\hat{D}(\Pi_1)\right],\end{aligned} \tag{11}$$

where $s_1\equiv\xi_1/R_0$, $s_2\equiv\xi_2/R_0$. Evaluating the right-hand sides of these equations in lowest order in $(1/n)$ and $x^2\ll 1$ (corresponding to an assumed localization) we obtain

$$\begin{aligned}&\frac{\partial}{\partial T_0}\xi_2(\vartheta,\alpha,T_0,T_1,\ldots,n)-\frac{1}{\rho_0 R_0^3}\hat{D}(\Pi_2)=0,\\ &\frac{\partial}{\partial T_0}\Pi_2(\vartheta,\alpha,T_0,T_1,\ldots,n)-\sigma\left(\nabla_s^2+2\right)\xi_2=\sigma n^2\left(\frac{n}{8R_0}\right)\cos(2n\alpha)\left(\tilde{\xi}_1 e^{-i\omega T_0}+\text{c.c.}\right),\end{aligned} \tag{12}$$

where we used the assumption given in (9c) regarding the scale of the time variation of the envelope. Note that resonant excitation of the second harmonic does not appear owing to the dispersion of the surface waves $(\sigma_{2n}^2-4\omega^2)\approx(\sigma_{2n}^2-4\sigma_n^2)=4\sigma_n^2$. Thus we find for the second order distortion

$$\begin{aligned}&\xi_2=\xi_2^0+\xi_2^2, \quad \xi_2^0=-\frac{n}{16R_0}\tilde{\xi}_1\tilde{\xi}_1^*\cos(2n\alpha), \quad \xi_2^2=\frac{n}{16R_0}\left(\tilde{\xi}_1^2 e^{-i2\omega T_0}+\text{c.c.}\right)\cos(2n\alpha),\\ &\Pi_2=\left(\frac{\sigma n^2}{\omega}\right)\frac{n}{16i R_0}\left(\tilde{\xi}_1^2 e^{-i2\omega T_0}-\text{c.c.}\right)\cos(2n\alpha).\end{aligned} \tag{13}$$

In a similar way, evaluating the right-hand sides of the third order equations we obtain

$$\begin{aligned}&\frac{\partial^2}{\partial T_0^2}\xi_3-\frac{\sigma}{\rho_0 R_0^3}\hat{D}\left(\nabla_s^2+2\right)\xi_3\\ &\quad=2i\omega\frac{\partial}{\partial T_1}\frac{(\tilde{\xi}_1 e^{-i\omega T_0}-\text{c.c.})}{2}\cos(n\alpha)-\omega_1^2\frac{17}{32}\left(\frac{n}{R_0}\right)^2|\tilde{\xi}_1|^2\frac{(\tilde{\xi}_1 e^{-i\omega T_0}+\text{c.c.})}{2}\cos(n\alpha)\end{aligned}$$

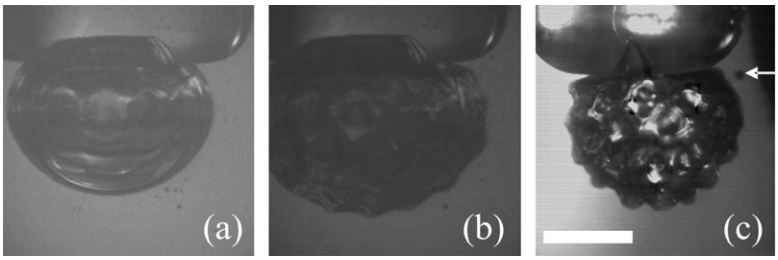

Fig. 2. The images show a bubble as the amplitude of excitation increases (a) 24 Pa, (b) 44 Pa, (c) 139 Pa (zero-to-peak). The mean radius of the bubble is ~ 2.1 mm and the scale bar in (c) is 2 mm. The driving field has frequency 1.506 kHz. See [13].

$$+\omega^2\left[\left(\frac{\omega_1^2}{\omega^2}-1\right)+\left(\frac{5}{8n}+\frac{3}{2}x^2\right)-\frac{3}{2n^2}\frac{\partial^2}{\partial x^2}\right]\frac{(\tilde{\xi}_1 e^{-i\omega T_0}+\text{c.c})}{2}\cos(n\alpha)+\{\text{non-secular terms}\}. \tag{14}$$

The evolution equation for the envelope $\tilde{\xi}_1$ results from the condition under which the secular forcing terms vanish in the third order equation. The final result is the nonlinear Schrödinger (NLS) equation

$$2i\omega\frac{\partial\tilde{\xi}_1}{\partial t}+\left(\omega_1^2-\omega^2\right)\tilde{\xi}_1+\omega_1^2\left(\frac{5}{8n}+\frac{3}{2}x^2\right)\tilde{\xi}_1-\frac{3\omega_1^2}{2n^2}\frac{\partial^2\tilde{\xi}_1}{\partial x^2}-\omega_1^2\frac{17}{32}\left(\frac{n}{R_0}\right)^2|\tilde{\xi}_1|^2\tilde{\xi}_1=0. \tag{15}$$

3. Self-focusing of Faraday ripples

From (15) we see that nonlinearity modifies the natural frequency according to

$$\omega_1^2\left(n,|\tilde{\xi}_1|^2\right)=\omega_1^2(n)-\frac{17}{32}\omega_1^2\left(\frac{n}{R_0}\right)^2|\tilde{\xi}_1|^2,$$

and the 'restoring' force will always be smaller in magnitude than for the linear case. The natural frequency of vibration is therefore decreased below its linear value and the stiffness will be reduced. Note that the same dependence is realized for surface waves on the flat surface [5].

The dispersion of the surface waves on the sphere deviates from that on the flat surface by the presence of the term proportional to x^2. This deviation can be ignored if the characteristic width of $\tilde{\xi}_1(x)-\Delta$ is smaller than $1/\sqrt{n}$. Alternatively, at $\Delta\sim 1/\sqrt{n}$ the term x^2 can be replaced by its mean value $\langle x^2\rangle$ within the localized envelope. For these cases the correction terms can be accounted for by renormalization of ω_1:

$$\omega_1^2\to\tilde{\omega}_1^2=\omega_1^2\left(1+\frac{5}{8n}+\frac{3}{2}\langle x^2\rangle\right).$$

In the static limit, Eq. (15) reduces to the Duffing equation, which is amenable to a solitary wave solution

$$\tilde{\xi}_1=\frac{\xi_m}{\cosh(x/\Delta)},\quad \xi_m=\frac{8R_0}{\sqrt{17}n}\left[\frac{\tilde{\omega}_1^2-\omega^2}{\tilde{\omega}_1^2}\right]^{1/2},\quad \Delta=\frac{1}{n}\left[\frac{3\tilde{\omega}_1^2}{2(\tilde{\omega}_1^2-\omega^2)}\right]^{1/2}. \tag{16}$$

The soliton amplitude ξ_m is inversely proportional to its width Δ as follows: $\xi_m=(3\cdot 32/17)^{1/2}(R_0/n^2)\Delta^{-1}$. The stability of the one-dimensional soliton envelope stems from the delicate balance of 'nonlinearity' and 'dispersion' in the NLS equation. Nonlinearity drives a solitary wave to concentrate further, whilst dispersion has the effect of spreading such a localized wave. If one of these two competing effects is lost, the soliton envelope becomes unstable and, eventually, cease to exist.

For the conditions of the experiment [1–3] a gas bubble is suspended beneath a glass surface, and pulsates as it is subjected to a sound field. The three images of Fig. 2 (see [13] for video) show a bubble as the amplitude of excitation increases. The amplitude of the radial pulsation (breathing mode) is too small to see, but Faraday waves can be seen. In Fig. 2(a), a localized mode around the bubble equator is excited. In Fig. 2(b), an increase in the amplitude of the driving acoustic field has caused a change in the pattern formed by parametrically excited Faraday waves. In Fig. 2(c), the nonlinearity is so high that the bubble fragments.

The amplitude of the breathing mode pulsation, which drives the nonlinearity, increases with increasing driving pressure and closeness of the driving frequency to the pulsation resonance. Given a fixed driving frequency, it follows from Fig. 2(a) that, for a sufficiently small driving pressure, only modes with a fixed m number $m=12$ participate in forming bubble distortion, and that these shape perturbations are localized near the equator. To clarify this selection in the generation of modes, we use an analogy with Faraday waves observed when a fluid layer with a free upper surface is subjected to vertical oscillation [3,12,13]. In order to demonstrate the implications of this work, the shape of the bubble distortions corresponding to the excitation of the solitary wave

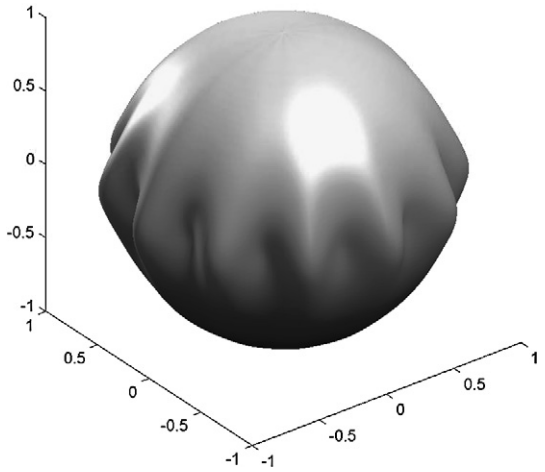

Fig. 3. The shape of the maximal distortion induced by soliton envelope.

with $|m| = 12$ has been evaluated. Fig. 3 shows the maximal distortion induced by a soliton envelope

$$\big[R_0 + \xi(\vartheta, \alpha)\big]/R_0 = 1 + \frac{\xi_m}{R_0} \frac{\cos(12\alpha)}{\cosh(\cos\vartheta/\Delta)},$$

calculated for $(\xi_m/R_0) = (3 \cdot 32/17)^{1/2} n^{-2} \Delta^{-1} = 0.1$ and $n = 12$. The soliton width is equal to $\Delta \approx 0.165$ in this case.

Comparisons between observation (as shown in Fig. 2) and dynamic modeling (as in Fig. 3) are as yet at an early stage. However, it is heartening to note the qualitative similarities, for example in that the peaks of the distortion are located at the equator, and furthermore that the width of this wave train in the polar-direction is smaller than the bubble diameter, but larger than the wave period.

4. Discussion

In this Letter we used an analogy between excitation of Faraday ripples in the channel and on a bubble wall and followed the approach derived by Larraza and Putterman [6]. In this manner, we analyzed an autonomous system, just as was done in [6]. It was shown by Miles [5] that accounting for dissipation and external driving does not change the structure of the soliton in a channel, but defines its amplitude and a phase. The form of these terms (damping and external driving) is also known for the parametrical excitation of ripples on the bubble wall (see the explicate form, for example, in [14]). The evolutionary equation (15) will be modified by the appearance of two additional terms $(2i\omega\delta\tilde{\xi}_1 + \beta\tilde{\xi}_1^*)$, where δ is the damping, β is the cofactor describing parametric interaction with the breathing mode and is proportional to the amplitude of this mode, and * denotes complex conjugation. The stationary solution of Eq. (15) accounting for damping and external driving still has a soliton-like form (16). The relation between the soliton's width Δ and the absolute value of its amplitude $|\tilde{\xi}_1|$ retains its autonomous form, but the phase and the modulus of $\tilde{\xi}_1$ are now determined by the frequency mismatch, damping and parametric driving. Because the structures of the solution of the autonomous and non-autonomous problems have the same appearance, this short communication has been limited to consideration of the elementary case which, however, gives correct representation of the general solution.

The theory outlined above is based on the isotropic model, but as is apparent from Fig. 2, the presence of a rigid wall violates this isotropy in the experimental system. The effect of a rigid wall to which the bubble adheres has been considered in [15,16]. For relatively small contact angles, corresponding to the conditions of the experiments discussed here, the analysis predicts a rather small ($\sim 25\%$) decrease in the natural frequency of the volume (breathing) oscillations and a smooth variation of the displacement amplitude along a bubble wall. The presence of the boundary does not render any significant influence on the surface modes with modes numbers (n, m): $(n - |m|)^2 \ll m^2$, $1 \ll m^2$, of which the solution localized near the equator is formed. The inequalities provide evidence for the feasibility of the condition (9b). These spherical harmonics vanish as one approaches along the meridians towards the poles. This circumstance is the physical basis for the localization of the Faraday ripples near the equator at low levels of excitation, since only these modes (from the multi-degenerated set of surface waves permitted by conditions of a parametrical resonance) do not interact with the boundary. Thus, the presence of the rigid wall is accounted for by the assumed form of the solution.

The defocusing of the Faraday ripples with increasing driving pressure (they completely cover the bubble surface in Fig. 2(b)) stems from the violation of resonance conditions due to the growing nonlinear shift of the natural frequency of the resonant mode. Further investigation will require knowledge of the stability domain of rolls and the presumed transition from rolls to squares (i.e., the transition from the pattern observed at Fig. 2(a) to the one observed at Fig. 2(b)) with increasing acoustic driving pressure. A further problem is the observation of the real two-dimensional solitons (or chain of such solitons) on the bubble wall which, like

the self-focused wave train considered in this Letter, will be localized not only in the transverse (meridian) direction but also in the direction of its phase velocity (i.e., along the equator).

5. Conclusions

In this Letter we considered oscillations of the bubble surface displacement in the form of a standing wave across the bubble equator modulated along the meridian. The nonlinear Schrödinger equation for the envelope of surface modes on the bubble wall has been obtained. The soliton solution of this equation describing self-focusing of Faraday ripples can explain why distortions observed in the experiment are located near the equator, and why the width of this wave train in the azimuth-direction is smaller than the bubble diameter, but larger than the wave period.

References

[1] P.R. Birkin, Y.E. Watson, T.G. Leighton, K.L. Smith, Langmuir Surfaces Colloids 18 (2002) 2135.
[2] Y.E. Watson, P.R. Birkin, T.G. Leighton, Ultrasonics Sonochem. 10 (2003) 65.
[3] T.G. Leighton, Int. J. Mod. Phys. B 18 (2004) 3267.
[4] J. Wu, R. Keolian, I. Rudnick, Phys. Rev. Lett. 52 (1984) 1421.
[5] J. Miles, J. Fluid Mech. 148 (1984) 451.
[6] A. Larraza, S. Putterman, J. Fluid Mech. 148 (1984) 443.
[7] V.E. Zakharov, J. Appl. Mech. Tech. Phys. 2 (1968) 190.
[8] T.B. Benjamin, P.J. Olver, J. Fluid Mech. 125 (1982) 137.
[9] T.B. Benjamin, J. Fluid Mech. 181 (1987) 349.
[10] A.O. Maksimov, in: A. Atchley, V. Sparrow, R.M. Keolian (Eds.), Innovations in Nonlinear Acoustics, AIP, New York, 2006, pp. 516–519.
[11] A.O. Maksimov, J. Exp. Theor. Phys. 106 (2) (2008) 355, Zh. Eksp. Teor. Fiz. 133 (2) (2008) 412 (in Russian).
[12] M. Faraday, Philos. Trans. R. Soc. London 121 (1831) 319.
[13] Video: http://www.isvr.soton.ac.uk/fdag/Faraday.htm.
[14] A.O. Maksimov, T.G. Leighton, ACUSTICA-Acta Acustica 87 (2001) 322.
[15] A.O. Maksimov, J. Sound Vibration 283 (2005) 915.
[16] A.O. Maksimov, T.G. Leighton, P.R. Birkin, in: A. Atchley, V. Sparrow, R.M. Keolian (Eds.), Innovations in Nonlinear Acoustics, AIP, New York, 2006, pp. 512–515.